Evidence for Cahill's dynamical space

Peter C. Morris

Adelaide, South Australia. March 6, 2018

E-mail: ptr.mrrs@tpg.com.au

It has been reported [1] that Random Event Generator (REG) devices can detect passage of dynamical 3-space waves. Herein we describe an attempt to find additional evidence for this discovery, using data from a REG located in Perth, Australia and from another in Manchester, U.K., for fifteen days centered on each full moon during a period of one year.

For each day we applied correlation analysis to determine travel times for putative waves. Then wave speed and direction, over each 24 hour period, were determined by fitting to the observed travel times, theoretical curves of how travel times would vary with Earth rotation. We thereby derived an average incoming RA, declination, speed and associated standard deviations for the waves of each day.

Following this we examined the directions and speeds to determine if they were consistent with a real physical phenomena, rather than being artifacts of random correlations. To this end we made use of probability density plots and other statistical techniques. On the way we recognized that wave orientation is not the same as 3-space flow direction and that it is the latter rather than the former which is of principle interest. Geometry implies that variation of flow speed will cause the detected speeds of wave fronts moving parallel to 3-space flow to have larger standard deviations than those moving across the flow. On this basis we preferentially selected the 50% of days with the largest speed standard deviations as being the more likely proxies for space flow direction.

A probability density plot of directions for these days exhibited a peak near $RA = 4.5\,h$, consistent with previous determinations of incoming 3-space flow direction by Reginald Cahill [3] and Dayton Miller [9]. Moreover, removing Earth orbital and gravitational inflow velocities from the observed velocities allowed a peak of higher density to be obtained, which is consistent with what one would expect of a real physical phenomena. The peak indicated a most probable galactic flow direction of $RA = 4.13\,h$, $dec = -77.8\,deg$ and wave speed of $505\,km/s$.

1 Introduction

In Cahill's theory of dynamical space [1], gravity is caused by acceleration of space into matter. The equations governing this process are nonlinear and nonlocal and predict fractal dynamical 3-space waves. These are a type of gravitational wave but differ from those predicted by General Relativity.

Random Event Generator (REG) devices generate random numbers by detecting the quantum to classical transition of electrons tunnelling through a barrier in a tunnel diode. According to the standard interpretation of quantum theory the transitions should be completely random, however Cahill's theory and experiments [1] suggest that this is not the case and that the transitions are driven by passage of dynamical 3-space waves. If so, then the random numbers output by different REG devices may not be 100% independent and correlation analysis of data from two spatially separated REG devices, approximately aligned with wave direction, should be able to reveal the travel time of waves that influence both devices.

To test this possibility we obtained data from a Global Consciousness Project [5] REG located in Perth, Australia and from another in Manchester, U.K. as shown in Table 1 for fifteen days centered on each full moon for all days for which data was available, from 26 June 2012 to 30 June 2013.

Of 195 potential days, complete data was available for 138.

Table 1: Details of GCP REG Devices Used

	Perth	Manchester
ID Number	2232	2006
Latitude	-31.921	53.682
Longitude	115.892	-2.165
Device Type	Orion	Orion

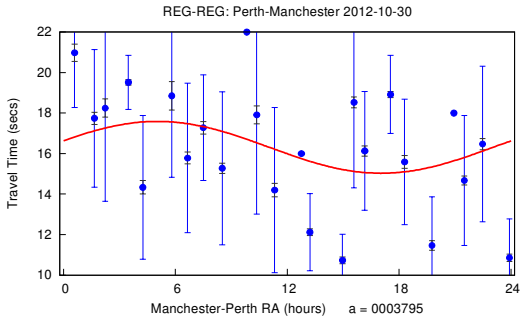

Fig. 1: Travel times from REG-REG Perth to Manchester data for October 30, 2012. High correlation values for each Manchester-Perth RA hour have been binned and the mean, SD (blue) and SEM (grey) shown. The red curve shows a least square error best fit of a sinusoid to all points. (Horizontal spacing of points is non-uniform because the RA of each point is the mean RA of values in the associated bin).

2 Travel times

For each of the 138 days, Perth to Manchester travel time τ values were determined by computing the correlation function,

$$C(\tau, t) = \sum_{t'=t-T}^{t'=t+T} S_1[t' - \lfloor \tau/2 \rfloor] \, S_2[t' + \lceil \tau/2 \rceil] \, e^{-a(t'-t)^2} \tag{1}$$

for data sequences $S_1[t]$ and $S_2[t]$ containing values output once per second by the REG devices. Here $\lfloor \, \rfloor$ and $\lceil \, \rceil$ represent floor and ceiling functions that round $\tau/2$ down or up to integer values to ensure correct indexing when τ is an odd number. $2T = 300s$ is the time interval used about UTC time t, and the Gaussian term applies a Gaussian window to suppress end effects. The width of this window is controlled by parameter a chosen as described in the following section.

τ values were determined by calculating $C(\tau, t)$ for τ in the range 9 to 23 seconds and then finding which value of τ in the range 10 to 22 corresponded to the maximum peak value of $C(\tau, t)$.

τ values with high correlations* were then binned and averaged per RA hour of the Manchester-Perth spatial separation vector that rotates with the Earth. We thereby obtained a mean travel time, Standard Deviation (SD) and Standard Error in the Mean (SEM) for 24 RA directions such as shown in Fig. 1.

3 Gaussian window parameter a

To determine an optimum value for Gaussian window parameter a, we histogrammed the binned values to obtain histograms such as shown in Fig. 2 and applied the following notion of signal visibility.

Let bar heights $y_1, y_2 \ldots y_N$ be the frequencies of τ values in columns $1, 2 \ldots N$. Then we can define signal visibility as mean deviation of bar height over mean bar height, ie.,

*For each day the high correlations were all those higher than a cutoff value which would allow each bin to contain at least one sample. To the bin(s) which then contained only one sample, a second sample with the nearest slightly lower correlation was added to allow calculation of standard deviation.

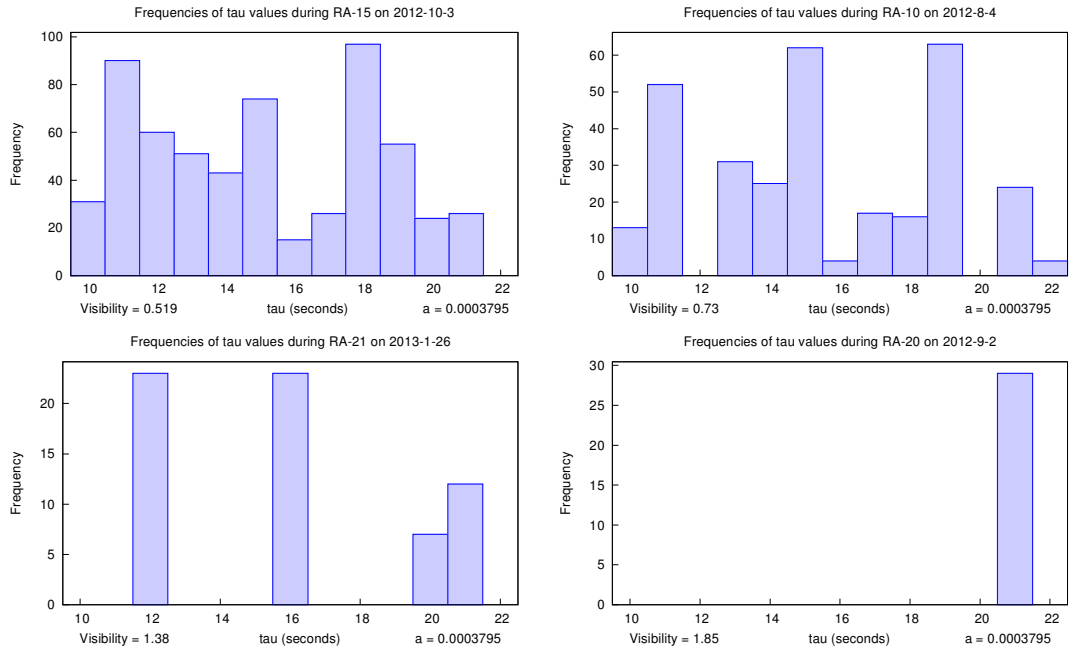

Fig. 2: Histograms of τ values detected during different RA hours illustrating a range of signal visibilities from low to high. The multiple peaks are consistent with passage of non-distinguishable wave forms, $w_n, w_{n+1}, w_{n+2}...$ etc. three to five seconds apart. Then the correlation of w_n at one detector with say w_{n+1} or w_{n+2} at the other, may be as large as the correlation with w_n. The single peak in the last histogram is consistent with passage of distinguishable waveforms.

$$V(y) = \frac{\frac{1}{N}\sum_{i=1}^{N}|y_i - \bar{y}|}{\bar{y}} \tag{2}$$

Applying this formula to a histogram containing equal numbers of bars with heights equal to max and min gives,

$$V = \frac{max - min}{max + min}$$

which is the formula for signal visibility used in interferometry. However, whereas the latter has a maximum value of $V = 1.0$ when $min = 0$, Eqn. (2) gives higher values when the number of maxima is reduced. Eg if a histogram contains one bar of height equal to max and $(N-1)$ with height of zero, then for our histograms with 13 bars (2) gives,

$$V(y) = 2\frac{N-1}{N} \approx 1.85$$

Using (2) we determined minimum visibility for each day and then the mean minimum for all days for a range of a values. The blue curve in Fig. 3. shows results obtained from data from seven days centered on each full moon during a year. This has a distinct peak at $a = 0.0003795$ so we used this value of a for subsequent calculations.

The red curve shows the mean for all days of the median standard error per day in the hourly τ values. This increases with a because increasing a reduces the width of the Gaussian window and reduces the number of correlation products that are averaging together, however the rate of increase shows a slight leveling off at peak visibility.

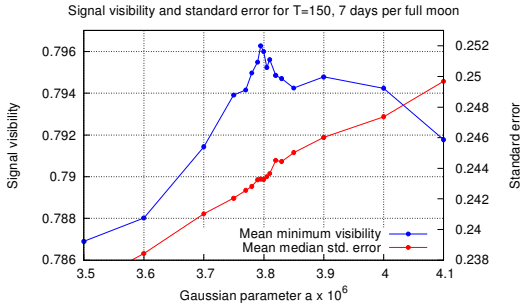

Fig. 3: Plots of mean minimum signal visibility and mean median travel time standard error for 7 days per full moon versus Gaussian window parameter a. The peak visibility occurs at $a = 0.0003795$.

4 Wave effects in histograms

The histograms of τ values shown in Fig. 2 illustrate a range of signal visibilities obtained during different RA hours. Histograms often had multiple peaks consistent with passage of similar wave forms, $w_n, w_{n+1}, w_{n+2}...$ etc. three to five seconds apart and which may have changed shape during passage from Perth to Manchester. Then the correlation of w_n at one detector with say w_{n+1} or w_{n+2} at the other, could be as large or larger than correlation with w_n. The presence of multiple peaks resulted in mean τ values with large standard deviations and also caused variation of the mean values to be attenuated towards the center of the 10 to 22 second detection range. To compensate for this we applied a disattenuation procedure to derived results as described later.

5 Fitting of sinusoids

Given travel time data for 24 RA directions, the incoming speed and the direction of plane waves can be determined by fitting,

$$\tau = \frac{\mathbf{R} \,.\, \mathbf{v}}{\mathbf{v}^2} \tag{3}$$

where $\mathbf{R}$ is the Manchester-Perth spatial separation vector and $\mathbf{v}$ is the velocity of the Earth relative to the waves. As the daily rotation of $\mathbf{R}$ causes the right hand side of Eqn. (3) to be sinusoidal, the fit can be done by fitting a sinusoid to the travel times such as shown in Fig. 1.

The RA of the peak will then indicate the incoming RA of the waves and the amplitude and mean will allow determination of incoming declination and speed. However, the means and amplitudes need to be adjusted to compensate for the above mentioned attenuation effect.

6 Amplitude disattenuation

When τ values obtained during a given RA hour are averaged together, the presence of multiple peaks in histograms such as seen in Fig. 2 implies that wrong values caused by miscorrelation will be averaged together with correct values and the resultant mean value will then most likely be attenuated towards the center of the detection range. If we assume such wrong values have a random distribution, this phenomenon will cause the amplitudes of the sinusoids to be attenuated by an amount equal to $1/(1 + n)$ where n is the average number of miscorrelation values per correct τ value.

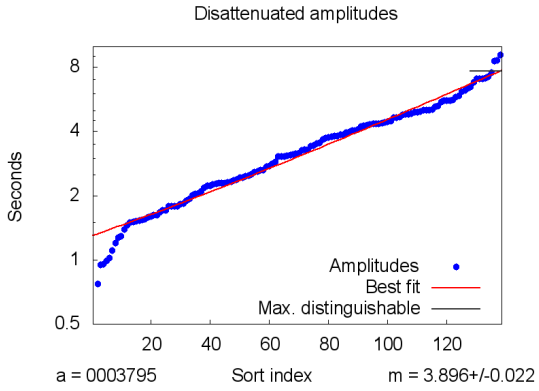

Fig. 4: Disattenuated amplitudes obtained by sorting the original values and then multiplying by a suitable value m to allow the best fit exponential curve to match the range of the detection process. Here use of a logarithmic vertical axis results in a straight line plot.

To compensate for this effect we multiplied the sinusoid amplitudes so that a best fit of an exponential curve to a sorted list of the multiplied values terminated at the amplitude of the largest sinusoid that could be fit to a waveform clipped to the τ range of 10 to 22. This "largest distinguishable amplitude" is 7.66. The exponential fit is shown in Fig. 4, where a logarithmic vertical axis makes it appear as a straight line plot. This resulted in a multiplier of $m = 3.896 \pm 0.022$.

It can be noted that this value corresponds to $n = (m - 1) \approx 2.9$ miscorrelation values per correct value.

7 Incoming declination and speed

If we let τ_{mean} and τ_{amp} be the mean and amplitude of each sinusoid fit, τ_{mid} be the center of the detection range and m be the disattenuation multiplier determined above, then the disattenuated mean value will be,

$$T_{mean} = \tau_{mid} + m(\tau_{mean} - \tau_{mid})$$

and the disattenuated amplitude will be $A = m\tau_{amp}$ and we can define,

$$T_{max} = T_{mean} + A$$

$$T_{min} = T_{mean} - A$$

Then if $\delta_{\mathbf{R}}$ and $\delta_{\mathbf{v}}$ are respectively the declinations of $\mathbf{R}$ and $\mathbf{v}$, then $\delta_{\mathbf{v}}$ can be found by numerically solving,

$$\frac{T_{min}}{T_{max}} = -\frac{cos(\delta_{\mathbf{v}} + \delta_{\mathbf{R}})}{cos(\delta_{\mathbf{v}} - \delta_{\mathbf{R}})} \tag{4}$$

And wave speed relative to Earth is then,

$$s = \frac{|\mathbf{R}|\, cos(\delta_{\mathbf{v}} - \delta_{\mathbf{R}})}{T_{max}} \tag{5}$$

8 Aberration of incoming wave velocity

Let $\mathbf{v}_G$ be the velocity of the Sun relative to distant galactic space, $\mathbf{v}_{inS}$ be velocity due to acceleration of space towards the Sun, $\mathbf{v}_{orbit}$ be the orbital velocity of the Earth and $\mathbf{v}_{inE}$ be velocity due to acceleration of

space towards the Earth. Then the velocity of a point on or within the Earth relative to incoming 3-space can be approximated by,

$$\mathbf{v} \approx \mathbf{v}_G - \mathbf{v}_{inS} + \mathbf{v}_{orbit} - \mathbf{v}_{inE} \tag{6}$$

Approximate vector addition of these components is possible because at the Earth's orbital positions, $\mathbf{v}_G$, $\mathbf{v}_{inS}$ and $\mathbf{v}_{orbit}$ are approximately orthogonal and $\mathbf{v}_{inE}$ represents a relatively small Earth directed effect. (Justification for vector addition of these components can be found in [4].)

From (6) it follows that if 3-space waves have a constant velocity relative to space and if $\mathbf{v}_{WG}$ is the velocity of the Sun relative to distant waves, then the velocity of a point on or within the Earth relative to incoming waves is,

$$\mathbf{v}_W \approx \mathbf{v}_{WG} - \mathbf{v}_{inS} + \mathbf{v}_{orbit} - \mathbf{v}_{inE} \tag{7}$$

which expresses how wave velocities are aberrated by the orbital and inflow velocities.

However the speeds that we derive from T_{max} in (5) correspond to *average* speeds of waves through deep paths through the Earth. Calculation of such speeds for the expected range of values of $\mathbf{v}_{WG}$, showed that the effect of higher speeds induced by $\mathbf{v}_{inE}$ along the downward portions of such a paths, would be almost exactly cancelled by the effect of lower speeds induced along the upward portions.

This implies that for average velocities $\mathbf{v}_{Wtt}$, derived from travel times through the Earth, (7) should be replaced by,

$$\mathbf{v}_{Wtt} \approx \mathbf{v}_{WG} - \mathbf{v}_{inS} + \mathbf{v}_{orbit} \tag{8}$$

ie. without the the $\mathbf{v}_{inE}$ term.

Then to remove the aberrating velocities and obtain $\mathbf{v}_{WG}$ from $\mathbf{v}_{Wtt}$ we can rearrange (8) as,

$$\mathbf{v}_{WG} \approx \mathbf{v}_{Wtt} + \mathbf{v}_{inS} - \mathbf{v}_{orbit} \tag{9}$$

9 Probability density plots of wave direction

Using the methods described above we calculated an incoming RA, declination, speed and associated standard deviations, for each of the 138 days.

The calculated directions are wave directions rather than 3-space flow direction, but waves travelling more or less parallel to 3-space flow will experience forward variations of speed in response to variations of flow speed, whereas those moving across the flow will merely be accelerated sideways. Then since flow speed has been reported to vary from hour to hour [1, 9] and since this is also consistent with predicted turbulence [4], the travel times of the former should exhibit greater variation than those of the latter.

So selecting waves that exhibit greater speed variation during each day should select waves that on average are closer to 3-space flow direction, To this end, we selected the 50% of wave velocities whose speeds exhibited the largest standard deviations. Figs. 5 and 6 show the difference this makes.

Fig. 5 shows a probability density plot of incoming directions for all days with a single peak near $RA = -5.0\,h$ which can be assumed to represent the average orientation of all waves, unrelated to space flow direction.

In contrast, Fig. 6, which shows incoming directions for the 50% of days with the largest speed standard deviations, shows two peaks, one corresponding to the above, and another near $RA = 4.5\,h$ which is consistent with previous determinations of incoming 3-space flow direction by Reginald Cahill [3] and Dayton Miller [9].

Moreover, if the velocities contributing to the peak near $RA = 4.5\,h$ are of physically real waves per dynamical 3-space theory, then they should have been aberrated by Earth orbital and Sun inflow velocities

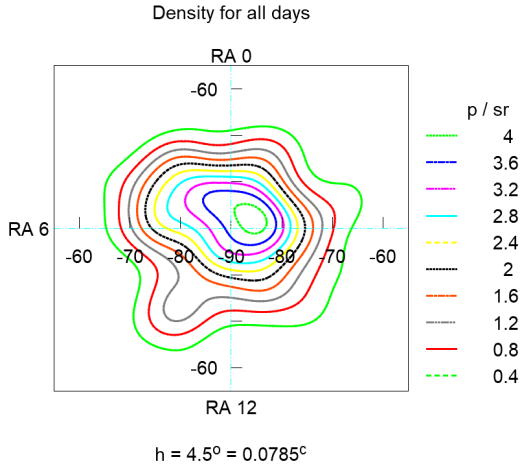

Fig. 5: Probability density of incoming wave directions for all days. (p/sr means probability per steradian and h is the bandwidth of the Gaussian kernel.)

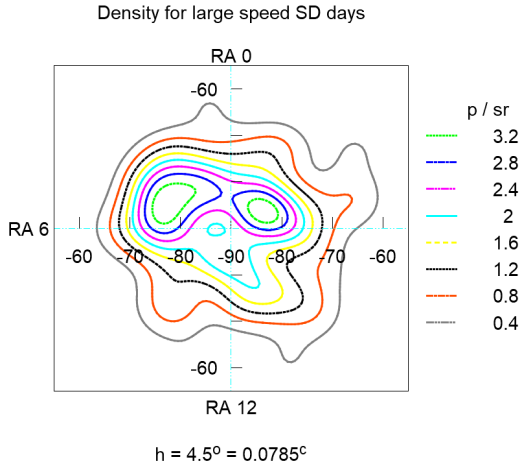

Fig. 6: Probability density of incoming wave directions for the 50% of days with largest speed standard deviations.

and so removing these velocities from the observed wave velocities should allow a higher peak to be obtained.

This turns out to be the case!

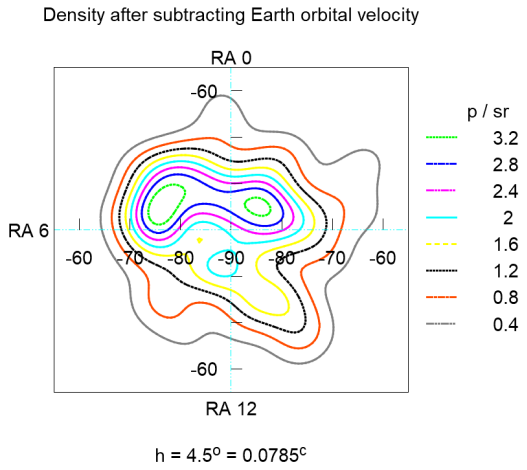

Fig. 7: Probability density after removing Earth orbital velocity only.

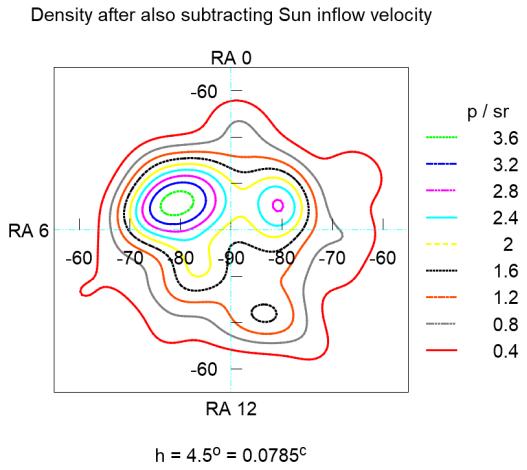

Fig. 8: Probability density after removing both Earth orbital and Sun inflow velocities.

Fig. 7 shows that removing Earth orbital velocity alone is not sufficient to demonstrate the expected effect. But Fig. 8 shows that removing the Sun inflow as well as the Earth orbital velocity increases the height of the peak near $RA = 4.5\,h$ from below 3.6 in Figs. 6 and 7 to above 3.6 in Fig. 8. (NB contours are colored from top down as the wxMaxima plotting software used did not allow bottom up coloring.)

By applying a search procedure to find the peak of Fig. 8, the highest probability density was found to be 3.82 at $RA = 4.13\,h$, $dec = -77.8^0$.

To find a speed, we applied a 3D kernel with an angular bandwidth centered on this direction to 138 velocities obtained by subtracting orbital and inflow velocities from all the available travel time wave velocities. (We used all available velocities, because the angular bandwidth reliably selects velocities relevant to the determined direction, whereas the method we used to select 50% as more likely to be

proxies for space flow direction would inevitably exclude some good values.) An angular bandwidth of 4.5^0 and a speed bandwidth of $40\,km/s$ then gave a peak of highest density at $505\,km/s$.

We take this direction and speed as our best estimate of $\mathbf{v}_{WG}$ that we defined as Sun velocity relative to distant galactic waves. As results depend on the proportion of days selected, we repeated calculations for the proportions shown in Table 2 and obtained reasonably stable results for proportions of 45% to 60%, but as 50% gave the highest density we took this as the optimum choice.

10 Confidence interval estimation

To estimate confidence intervals for the RA and declination of the peak density shown in Fig. 8, we applied bootstrap resampling [6] to the 69 wave directions chosen as proxies for flow direction. To do this we repeatedly made a random selection of 69 directions from the original 69 and then found the peak density for this random set.

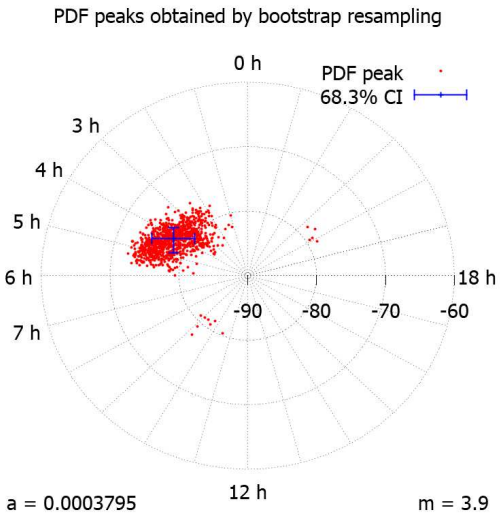

Fig. 9: Example of 1000 applications of bootstrap resampling. Each point shows a peak of probability density calculated from a different set of 69 wave directions randomly selected from the 69 observed directions.

Repeatedly applying this procedure gave multiple estimates of RA and declination from which we calculated 68.3% confidence intervals. Fig. 9 shows an example of results obtained from one thousand iterations.

Ten thousand iterations gave $RA = 4.13^{+0.80}_{-0.89}\,h$, and $dec = -77.8^{+2.7}_{-2.1}\,deg$.

Applying a similar procedure to wave speed for this direction gave $505^{+11}_{-8}\,km/s$.

Table 2: Peak density and associated values

Days selected	Peak density (p/sr)	RA (hrs)	dec (deg)	speed (km/s)
45%	3.78	4.35	-77.5	504
49%	3.72	4.27	-76.9	504
50%	3.82	4.13	-77.8	505
51%	3.76	4.13	-77.8	505
55%	3.54	4.07	-78.1	505
60%	3.51	3.79	-78.9	507

11 RA probability calculation

Having obtained an estimate of $\mathbf{v}_{WG}$, we can use Eqn. (8) to predict the most probable values of incoming wave direction and speed $\mathbf{v}_{Wtt}$ that would be observed by the REG devices at different times of the year. The red curve in Fig. 10 shows predicted RA while the points show the RAs of the 69 incoming wave velocities selected as more likely to be proxies for 3-space flow direction.

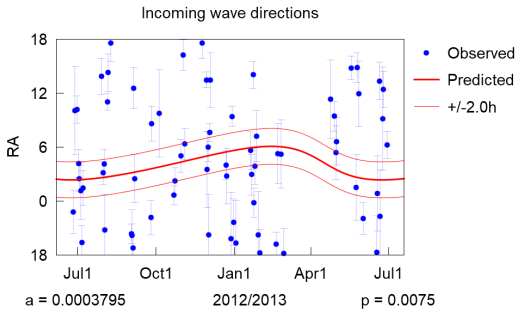

Fig. 10: Points show the RAs of 69 incoming wave directions selected as more likely to be proxies for 3-space flow direction. The red curve shows RA values obtained from Eqn. (8) using our estimate of $\mathbf{v}_{WG}$ with $RA = 4.13\,h$, $dec = -77.8^0$ and $speed = 505\,km/s$. Of 69 points, 20 lie within ± 2.0 RA hours of this curve. The probability of this degree of closeness arising from chance is $P = 0.0075$.

Inspection of Fig. 10 reveals that 20 of the 69 points lie within ± 2.0 RA hours of predicted RA. However if the RAs were random, axial symmetry would imply a uniform distribution and we would expect only $69 \times \frac{4.0}{24} = 11.5$ points to lie this close to the curve.

We therefore checked the probability of the observed distribution being due to chance using the formula,

$$P = \sum_{k=r}^{n} \binom{n}{k} p^k (1-p)^{n-k} \tag{10}$$

where $r = 20$ is the number of points within ± 2.0 RA hours of the curve, $n = 69$ is the total number of points and $p = 4.0/24$ is the probability of a point lying within ± 2.0 RA hours of the curve if the distribution of RAs was random and uniform.

Inserting these figures gives $P_{RA} = 0.0075$.

12 Declination probability calculation

Since the derivations of the declinations and RAs are mutually independent, we can validly make an independent check of the probability of the derived declinations. The points in Fig. 11 show the twenty incoming wave directions whose RAs in Fig. 10 were within $\pm 2.0\,h$ of predicted RA. The blue orbital aberration ellipse shows predicted RA and declination over the course of a year calculated using Eqn. (8) with our estimate of $\mathbf{v}_{WG}$.

Of the twenty points, the seven shown as solid have declinations that lie within $\pm 1.49^0$of the predicted values.

This prompts the question, "If the declinations of the points were from a random distribution, what is the probability that seven out of twenty would lie this close to their predicted declination?"

To answer this we first used the declinations of our entire set of 138 wave velocities to derive the declination cumulative distribution function shown in Fig. 12.

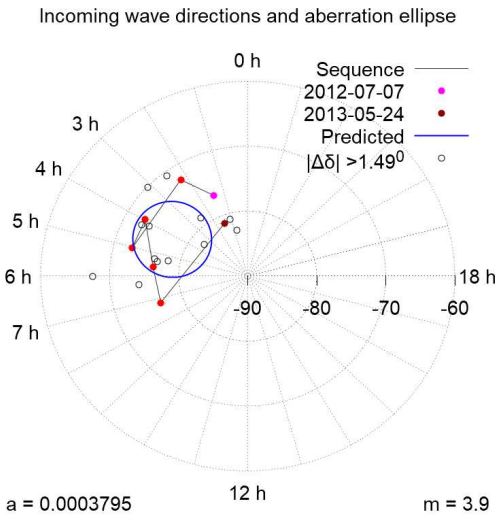

Fig. 11: Points show the twenty incoming wave directions whose RAs in Fig. 10 are within $\pm 2.0\,h$ of predicted RA. The blue orbital aberration ellipse shows variation of predicted RA and declination during a year due to the combined effect of Earth orbital and Earth and Sun inflow velocities. Of the twenty points, the seven shown as solid have declinations that lie within $\pm 1.49^0$of predicted values. The probability of this closeness being a result of chance is $P_{dec} = 0.0088$.

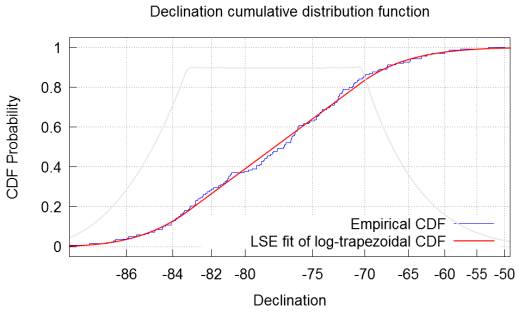

Fig. 12: Cumulative distribution function derived from 138 declinations

Then for each of the seven points, we used this function to calculate the probability that a declination drawn at random from the distribution would be as close as observed to the predicted value. We then took the maximum probability as a conservative probability for all seven points. This maximum probability turned out to be 0.1262 and was for the maximum deviation of $\pm 1.49^0$

We could then reapply Eqn. 10 where this time $r = 7$ is the number of points with declinations within $\pm 1.49^0$ of their predicted value, $n = 20$ is the total number of points and $p = 0.1262$ is the maximum probability of a point having a declination within $\pm 1.49^0$ of its predicted value if the declinations were drawn at random from the above distribution.

Inserting these figures gives $P_{dec} = 0.0088$.

13 Joint probability

Since the RAs and declinations were independently derived, the joint probability that the closeness of their observed values to their predicted values could have arisen by chance is $P = P_{RA} \times P_{dec} = 0.0075 \times$

0.0088,

which gives,

$$P < 6.7 \times 10^{-5}$$

14 Comparison with related results

Table 3 shows a comparison between two values of $\mathbf{v}_{WG}$ reported in this paper and in [2] and a value of $\mathbf{v}_G$ reported by Cahill in [3]. To determine $\mathbf{v}_{WG}$ from wave velocities, we attempted to select velocities that would be approximate proxies for 3-space flow direction. In view of this, the directions of the two values of $\mathbf{v}_{WG}$ should approximately match the direction of $\mathbf{v}_G$. Looking at the table it is clear that all three RAs match to within the 68.3% CIs while the CI for the declinations of "This paper" is nearly large enough to encompass the other declinations.

We don't expect the speeds of $\mathbf{v}_{WG}$ to match that of $\mathbf{v}_G$ because we expect the waves to be travelling through 3-space with some non-zero speed, but the small difference between the speeds suggests that propagation speed is low.

Table 3: Comparison of related results

Ref.		RA (hrs)	dec (deg)	speed (km/s)
This paper	$\mathbf{v}_{WG}$	$4.13^{+0.83}_{-0.81} prob$,	$-77.8^{+2.7}_{-2.1}$	505^{+11}_{-8}
Morris [2]	$\mathbf{v}_{WG}$	4.00 ± 0.51	-79.8 ± 1.0	500 ± 113
Cahill [3]	$\mathbf{v}_G$	4.29	-75	486

15 Conclusions

In this paper we have presented results that illustrate correlations between widely separated Random Event Generator devices that appear to be caused by a cosmic scale wave phenomenon. Our analysis and probability calculations suggest that it is very unlikely that our results could be a result of chance and much more likely that they are evidence for a genuine physical effect. To interpret and analyse our data we applied Cahill's theory of dynamical 3-space and found that this allowed us to obtain intelligible results consistent with the theory. This does not prove the theory is correct, but it would seem to be good evidence for the theory.

Other possibilities are that the REG devices might be detecting passage of the Earth though holographic [9] or fractal [10] spacetime structures.

Acknowledgements

Special thanks are owed to GCP [5] and its director Dr. Roger Nelson for enabling access to valuable data from the GCP network of REG devices.

Thanks to Pierre Millette for helpful suggestions with respect to earlier work leading to this paper.

References

[1] Cahill R.T. Nanotechnology Quantum Detectors for Gravitational Waves: Adelaide to London Correlations Observed. *Progress in Physics*, 2013, v. 4, 57-62.
http://www.ptep-online.com/2013/PP-35-09.PDF

[2] Morris P.C. Estimating 3-Space Velocity from REG-REG Correlations http://vixra.org/abs/1604.0352

[3] Cahill R.T. Combining NASA/JPL one-way optical-fiber light-speed data with spacecraft Earth-flyby Doppler-shift data to characterise 3- space flow. *Progress in Physics*, 2009, issue 4, 50-64.
http://www.ptep-online.com/2009/PP-19-05.PDF

[4] Cahill R.T. The dynamical velocity superposition effect in the quantum-foam theory of gravity. In: *Relativity, Gravitation, Cosmology: New Developments*, Dvoeglazov V., ed., Nova Science Pub., New York, 2009.
https://arxiv.org/abs/physics/0407133

[5] The Global Consciousness Project http://global-mind.org/

[6] Hesterberg T. What Teachers Should Know About the Bootstrap: Resampling in the Undergraduate Statistics Curriculum *Am Stat.* 2015 Oct 2; 69(4): 371–386.

[7] J René van Dorp and Samuel Kotz. Generalized Trapezoidal Distributions. *Metrika*, 58(1):85–97, 2003.

[8] Bannister R.N. A guide to computing orbital positions of major solar system bodies: forward and inverse calculations
http://www.met.rdg.ac.uk/%7Eross/Documents/OrbitNotes.pdf
http://www.met.rdg.ac.uk/%7Eross/Astronomy/Planets.html

[9] Miller D.C. The Ether-Drift Experiment and the Determination of the Absolute Motion of the Earth *Rev. Mod. Phys.* 5, 203 – Published 1 July 1933.

[10] Rabounski D. and Borissova L .General Relativity Theory Explains the Shnoll Effect and Makes Possible Forecasting Earthquakes and Weather Cataclysms *Progress in Physics*, 2014, issue 2, 63-70.

[11] Scale Relativity and Fractal Space-Time: Theory and Applications *Found.Sci.15:101-152,2010*